Earth and Planetary Science Letters 576 (2021) 117216

Contents lists available at ScienceDirect

Earth and Planetary Science Letters

www.elsevier.com/locate/epsl

Impact-related crystallization and modification of small zircons in Apollo 15 and 16 impactites at 4.2 Ga

Dennis Marcel Vanderliek [a,*], Harry Becker [a], Alexander Rocholl [b]

[a] Institut für Geologische Wissenschaften, Freie Universität Berlin, Malteserstraße 74-100, 12249 Berlin, Germany
[b] Deutsches GeoForschungsZentrum GFZn, Telegrafenberg, D-14473 Potsdam, Germany

ARTICLE INFO

Article history:
Received 17 February 2021
Received in revised form 10 September 2021
Accepted 17 September 2021
Available online 8 October 2021
Editor: W.B. McKinnon

Keywords:
Moon
Impact
Zircon
Apollo 15
Apollo 16
U-Pb Geochronolgy

ABSTRACT

Because of their robustness against resetting, *in situ* U-Pb ages of zircons in lunar impactites have the potential to provide constraints on the lunar bombardment history that may complement the more common K-Ar ages. Most previous work has focused on relatively large zircons that show growth zoning and ages were mostly interpreted as early igneous crystallization ages. Here we combine high-resolution mineralogical imaging and *in situ* U-Pb dating by ion microprobe to identify, characterize and date <20 µm size zircons in thin sections of lunar impact breccias. Several tens of grains of zircons of this size range were identified in thin sections of impactites from the Apollo 15 and 16 landing sites. Small zircons are more abundant in both noritic and evolved clinopyroxene, SiO_2 or K-feldspar bearing lithologies compared to anorthositic bulk compositions. Both granular zircon aggregates and overgrowth on existing zircon or baddeleyite (in breccias 15455 and 67915) are interpreted to reflect high-temperature recrystallization of zircons or its high-temperature-pressure precursor phases, following shock heating events by impact. In contrast, conchoidal or poikilitic zircons <10 µm in Fe-Ni metal bearing noritic clasts or matrix (67915, 67955) crystallized *in situ* from impact melt. Most U-Pb ages of the 24 analyzed grains are either concordant or reverse discordant with ^{207}Pb-^{206}Pb ages ranging from 4.15 to 4.25 Ga. The small age range, combined with a large textural spectrum and the frequent presence of Fe-Ni metal suggest zircon crystallization from impact melt and recrystallization of pre-existing zirconium-bearing minerals by impact heating. Such 'impact' zircons with 4.2 Ga ages have now been reported from most Apollo landing sites, suggesting widespread formation and modification of zircons by basin-forming impacts at this time. The contrast between U-Pb zircon (predominantly 4.2 Ga) and K-Ar feldspar ages (predominantly 3.9 Ga) likely reflects resetting of the latter chronometer by impact heating.

1. Introduction

Early isotopic dating and prevalence of isotopic ages of 3.95 to 3.85 Ga obtained by the K-Ar and Rb-Sr decay systems at the Apollo landing sites led to the hypothesis of a spike in the impactor flux in the inner solar system, referred to as terminal lunar cataclysm or late heavy bombardment (LHB) (Ryder, 2002; Stöffler et al., 2006; Tera et al., 1974). This contrasts with crater counting model ages (e.g. Neukum and Ivanov, 1994) suggesting that many of the large lunar basins were formed prior to 4 Ga and that an exponential decay of the accretion flux after formation of the terrestrial planets may be more appropriate. The latter view is supported by refined crater counting work on lunar terranes which was unable to confirm hints for more than one impactor population (Orgel et al., 2018). Recent isotopic dating studies concluded that the interpretation of isotopic ages of Apollo rocks may be biased due to resetting of the K-Ar feldspar chronometer by subsequent impacts and/or by an overall sampling bias at Apollo landing sites caused by abundant impactites with ejecta from the ~3.9 Ga old Imbrium basin (e.g. Fernandes et al., 2013; Norman et al., 2010; Grange et al., 2011).

Due to its high closure temperature of >900 °C (Cherniak and Watson, 2001) the U-Pb zircon chronometer is more robust against resetting by later heating events than other geochronometers. Because of their stability during intense brecciation or moderate heating, lunar zircons appear to conserve information on early igneous processes (e.g. Nemchin et al., 2012) and, in some cases, also the lunar bombardment history prior to 4.0 Ga (e.g. Crow et al., 2017 and references therein). Unfortunately, zircons in lunar impactites appear to be rare and require careful documentation of

* Corresponding author.
E-mail address: dennisvdl@zedat.fu-berlin.de (D.M. Vanderliek).

https://doi.org/10.1016/j.epsl.2021.117216

their textural relationship to interpret their ages either by primary igneous crystallization from lunar magmas or impact-related heating and crystallization in impact melts.

Clasts of primary igneous zircon in impactites are assumed to derive from ancient, KREEP rich rocks and have formed as early as 4.35 Ga (Borg et al., 2015; Nemchin et al., 2012). Continuous bombardment may have caused grain size reduction and destruction of zircon by impact-induced melting of earlier ejecta over time in lunar surface materials (Liu et al., 2020). Re-melting of KREEP-rich lunar surface materials by impacts and local differentiation of large impact melt sheets have led to local crystallization of zirconium-bearing minerals such as zirconolite, and presumably also zircon and baddeleyite that can be used to date the impacts responsible for the melt sheets (e.g. Norman and Nemchin, 2014; Norman et al., 2016). Some zircons in breccias may also have recrystallized at high temperatures due to impact-related heating (Crow et al., 2017; Nemchin et al., 2008).

Igneous zircons have commonly been identified by their strong zoning using cathodoluminescence (Grange et al., 2013; Thiessen et al., 2019, 2018; Meyer et al., 1996; Nemchin et al., 2009). The only zircon textures from lunar rocks that unambiguously can be ascribed to impact-related recrystallization are granular zircon aggregates (sometimes referred to as polycrystalline zircon (Crow et al., 2017); Grange et al., 2009; Thiessen et al., 2019; Grange et al., 2013), similar to granular zircons known from terrestrial impactites (e.g. Cavosie et al., 2018). Further zircon textures interpreted to have formed by impacts, are poikilitic (e.g. Liu et al., 2010) and acicular zircons (e.g. Grange et al., 2009) and those showing recrystallized rims (e.g. Bellucci et al., 2016; Pidgeon et al., 2007).

Previous studies frequently have analyzed relatively large lunar zircon grains, often as grain mounts and thus apart from their original context. The present study focuses on very small grains and their mineralogical and textural environments in three different types of impactites from the Apollo 15 and 16 landing sites. The identification of very small zircon grains and study of their petrographic context was made possible by application of an automatic mineralogical mapping method of thin sections at $\leq$ 4 µm resolution. So far, this tool has not been used in isotopic dating work of lunar breccias. Here, we report the discovery of a significant number of small (<20 µm) zircons, some of which were dated *in situ* by SIMS (secondary ionization mass spectrometry).

Using these tools, several objectives will be pursued: First, identification of criteria, which link small zircons in lunar impactites to impact heating or impact melt. Second, study of the effects of heating by later impact melt veins on the U-Pb system in older zircons from nearby clasts. Third, the influence of impact related heating on U-Pb age distributions from zircons in comparison to published K-Ar dates. The three samples studied here, represent a range of breccia lithologies of noritic to anorthositic composition, which have been shown to record evidence for heating at ~3.9 Ga caused by the Imbrium impact event. Our study also provides a larger number of U-Pb ages of unambiguously impact-generated zircons from the Apollo 16 landing site, allowing comparison of U-Pb zircon impact ages of all landing sites.

Although zircons from this study show a wide range in textures and petrogenetic context, they all indicate similar ages of ~4.2 Ga. Textures and phase assemblages suggest an impact-related origin of most of the small zircon grains. On the other hand, none of the zircons show ages of ~3.9 Ga or younger, suggesting robustness of the U-Pb system in zircon against subsequent heating by mixing with younger ejecta deposits.

2. Samples and methods

The well-studied breccias 15455 and 67955 are relatively simple lithologies, which differ in their formation history. In contrast, 67915 is a complex breccia with a highly diverse clast population that includes clasts with a mineralogy similar to clasts in 15455 and 67955, but also other compositions (Supplementary Figures S1 and S2).

2.1. Apollo 15 breccia 15455

Dimict breccia 15455 (sections ,27 and ,28) from Spur crater rim (Apollo 15, Station 7) comprises a light colored, brecciated, 'pristine' anorthositic norite breccia intruded by black impact melt veins. The qualification "pristine" stems from the low highly siderophile element (HSE) abundances of the norite, whereas the melt portion shows high HSE abundances and thus was contaminated by impactor material (Warren and Wasson, 1979; Liu et al., 2015), The black, clast rich glass in 15455 was interpreted as Imbrium impact melt (Ryder and Bower, 1977; Ryder and Wood, 1977), based on disturbed ^{40}Ar-^{39}Ar spectra with apparent dates between 3.82 Ga to 3.94 Ga (Alexander Jr. and Kahl, 1974; Bernstein, 1983; Shih et al., 1993), the geologic setting and its KREEP bearing composition (Lindstrom et al., 1988). Crow et al. (2017) separated granular aggregates of zircon (e.g. ~30 µm ø) that yielded Pb-Pb ages from 4.2 to 4.33 Ga and were interpreted to have formed by impact heating, however, the petrologic context of the zircons is unknown. This sample was selected, to study the zircons in the thin section and to test the sensitivity of the U-Pb system in zircon to resetting in proximity of the Imbrium melt veins.

2.2. Apollo 16 breccias 67955 and 67915

67955 and 67915 are breccias with high HSE abundances. They were chipped from a white clast from Outhouse rock (Meyer, 2005) at Station 11 at North Ray Crater. The KREEP poor samples and their host rock may derive from the Descartes formation, which presumably represents ejecta from deeper in the transient cavity of the Imbrium basin (Meyer, 2005; Norman et al., 2010). 67955 represents a cataclastic breccia consisting of noritic anorthosite clasts and a finer brecciated matrix that locally contains glass veins. Section ,48 contains a darker, more strongly brecciated domain with somewhat higher orthopyroxene and olivine fractions and a lighter colored domain. The rock was interpreted as a cumulate, formed from KREEP rich impact melt during a basin-scale impact event at ~4.2 Ga that has been re-heated at ~3.9 Ga during entrainment in ejecta material (Sm-Nd isochron and ^{207}Pb-^{206}Pb dates on zirconolite and apatite, (Norman and Nemchin, 2014; Norman et al., 2016). Because of the detailed previous work, 67955 is an excellent sample for comparison with U-Pb dates of zircon.

67915 (sections ,76 and ,84) is a fractured polymict impact breccia consisting of a fine-grained matrix containing different types of lithic and mineral clasts cross cut by veins of glass (Butler, 1972). The lithic clasts comprise ferroan anorthosite, noritic anorthosite, troctolitic anorthosite, sodic ferro-gabbro and ferroperidotite and the bulk composition corresponds to a KREEP-poor noritic anorthosite (Marti et al., 1983; Roedder and Weiblen, 1974; Taylor et al., 1980). Various clasts have been dated using the ^{40}Ar-^{39}Ar method yielding variably disturbed spectra and dates ranging from 3.71 Ga to 4.03 Ga (Kirsten et al., 1973; Marti et al., 1983; Venkatesan and Alexander Jr., 1976; Taylor et al., 1980). This sample was selected to test if U-Pb ages in zircon can be linked with specific clast lithologies in complex breccias.

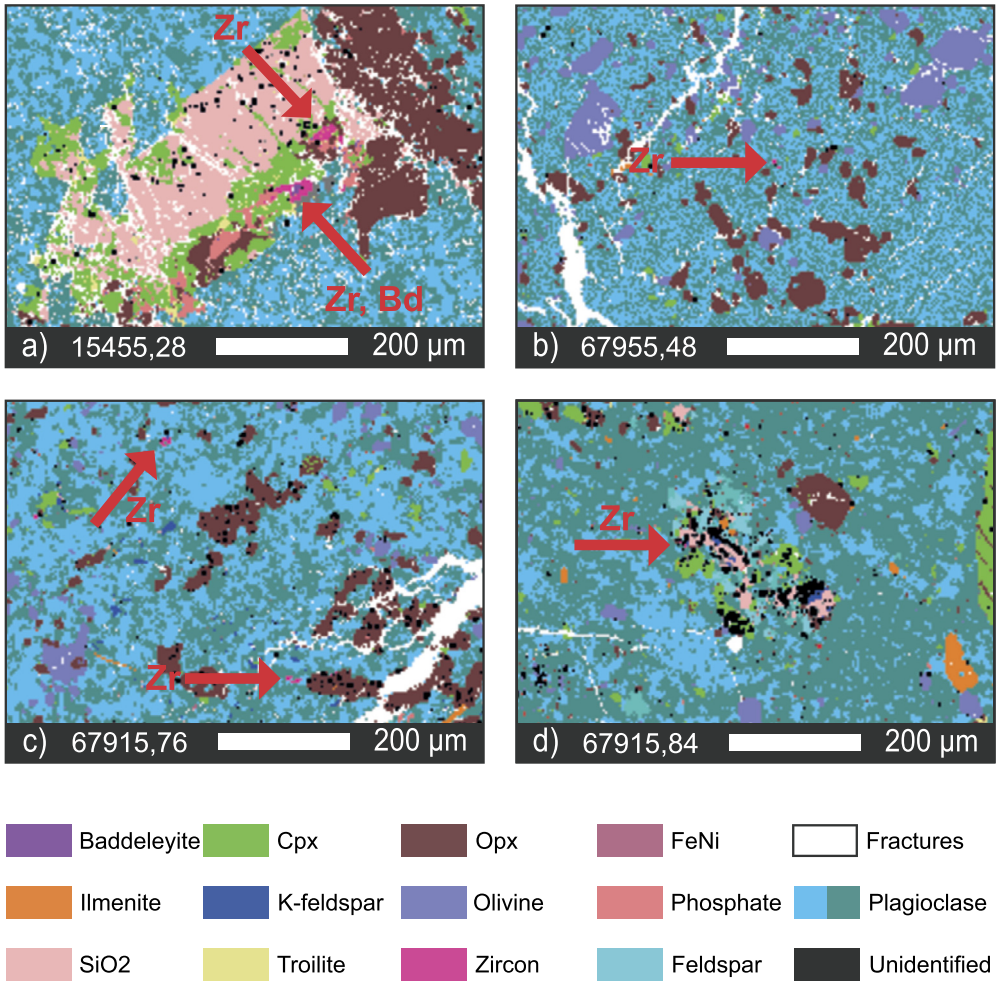

Fig. 1. QEMSCAN mineral maps showing the petrographic context of zircon (pixel size = 3.7 µm). The different colors of plagioclase reflect differences in anorthite component (An). The light blue represents high An content in the range of anorthite while the darker color represents lower An in the range of bytownite. Differences in An content often allow to distinguish clasts from matrix or from other lithologies e.g. impact melt. Since this method is semi-quantitative we only refer to plagioclase but show both colors. a) Granular zircons #11-1 (top) and #14-32, #14-3 (bottom) associated with baddeleyite and Ca-phosphate in a silica-diopside aggregate in a pristine norite portion of 15455,28. The assemblage is located 400 µm away from a vein of former impact melt. b) Zircon #17-1 in a noritic anorthosite clast in 67955,48. c) Zircons #41-1 (top) and #48-1 (bottom) from the same noritic anorthosite clast of 67915,76. d) Zircons #37-2 and #38-3 in a SiO_2 and K-feldspar bearing clast in 67915,84. (For interpretation of the colors in the figure(s), the reader is referred to the web version of this article.)

2.3. Analytical methods

Thin sections were mapped using back scattered electron imaging (BSE) at the GeoForschungsZentrum Potsdam using a and ZEISS Ultra Plus Scanning Electron Microscope. Mineralogical maps of sections were generated using Quantitative Evaluation of Minerals by Scanning Electron Microscopy (QEMSCAN) at the Institute for Geology of the RWTH Aachen. Secondary X-rays and back scattered electrons were detected by a Bruker Dual X-Flash 5030 energy-dispersive X-ray spectroscopy detector. By comparing the acquired spectra with customized libraries, mineral phases were semi-automatically assigned to each position of measurement (Gronen et al., 2019; Sindern and Meyer, 2017). A step size of 3.7 µm for scanning positions was used resulting in corresponding pixel based mineral phase maps of thin sections (e.g. Fig. 1). BSE images of section domains displayed in Fig. 1 are shown in Supplementary Fig. S3.

To prepare for SIMS analysis, the carbon coating was removed from the thin sections using 0.3 µm aluminum oxide powder and ethanol, followed by a treatment with ethanol in an ultrasonic bath for three minutes to remove surface contaminants. Afterwards the sections were gold coated (35 nm). Determinations of Pb/U ratios and isotopic composition of spots on selected grains were performed using a CAMECA IMS 1280 HR SIMS at the GeoForschungszentrum Potsdam. A high spatial resolution was reached by adjusting apertures to allow a spot of the primary O_2^- beam with a diameter of ~5 µm applying a primary high voltage of −13 kV. The nominal mass resolution of the mass spectrometer was set to 4000 – 4100 at 10% peak height (M/ΔM). Beam currents were 0.21 – 0.25 nA (67955), 0.19 – 0.22 nA (15455) and 0.14 – 0.22 nA (67915). Pre-sputtering was performed for 80 to 240 s. The U-Pb ratios in the unknowns were calibrated against the zircon reference material 91500 (Wiedenbeck et al., 1995). Reference materials were measured on separate mounts, possibly causing the partial reverse discordance observed for some analyses (Nemchin et al., 2008). Calibration of the sample data was performed by session using SIMS data reduction spreadsheets, followed by further processing using Isoplot 4.15 (Ludwig, 2011). Ages were calculated assuming a $^{238}U/^{235}U$ of 137.818 (Hiess et al., 2012). Four analyses (see Table 1 and Results) have been common Pb corrected using the model of Stacey and Kramers, 1975, assuming that all common Pb reflects terrestrial contamination. The labeling of zircon analyses is explained in Supplementary Information 1.

Table 1
U-Th-Pb isotopic data of zircons of samples 15455,27 and 15455,28.

Sample	Grain	Spot	U [ppm]	Th [ppm]	Pb [ppm]	238U/204Pb	238U/206Pb	±2σ (%)	204Pb/206Pb	±2σ (%)	207Pb/206Pb	±2σ (%)	207Pb*/206Pb	±2σ (%)	207Pb*/206Pb	±2σ (Ma)
15455,27	30-1	1	185	63	261	$1.65*10^{9}$	1.12	4.1	$7*10^{-10}$	200	0.49	1.0	0.49	1.0	4201	15
15455,27	30-1	2	176	129	276	$1.06*10^{9}$	1.06	4.1	$1*10^{-09}$	200	0.4876	0.9	0.4876	0.9	4204	14
15455,27	12-2	1	273	155	729	$1.672*10^{9}$	0.60	18.1	$4*10^{-10}$	200	0.4892	0.8	0.4892	0.8	4209	12
15455,27	12-2	2	163	61	229	$1.14*10^{9}$	1.14	3.8	$1*10^{-09}$	200	0.4895	0.9	0.4895	0.9	4210	14
15455,28	14-3	1	342	231	626	$1.73*10^{9}$	0.90	4.1	$5*10^{-10}$	200	0.4839	0.9	0.4839	0.9	4193	14
15455,28	14-32	1	258	133	386	$1.59*10^{9}$	1.08	3.3	$7*10^{-10}$	200	0.4863	0.9	0.4863	0.9	4200	13
15455,28	14-32	2	242	152	385	$1.03*10^{9}$	1.03	3.3	$1*10^{-09}$	200	0.4827	0.8	0.4827	0.8	4189	12
15455,28	11-1	1	183	103	290	$1.03*10^{9}$	1.03	3.4	$1*10^{-09}$	200	0.4799	1.1	0.4799	1.1	4181	16
15455,28	11-1	2	340	157	532	$1.02*10^{9}$	1.02	3.4	$1*10^{-09}$	200	0.4714	0.8	0.4714	0.8	4154	12
15455,28	22-6	1	170	66	271	$1.454*10^{9}$	0.99	3.2	$7*10^{-10}$	200	0.48	1.2	0.48	1.2	4168	18
15455,28	29-1	1	202	55	309	$1.02*10^{9}$	1.02	3.4	$1*10^{-09}$	200	0.48	1.0	0.48	1.0	4184	15

* Common Pb corrected.

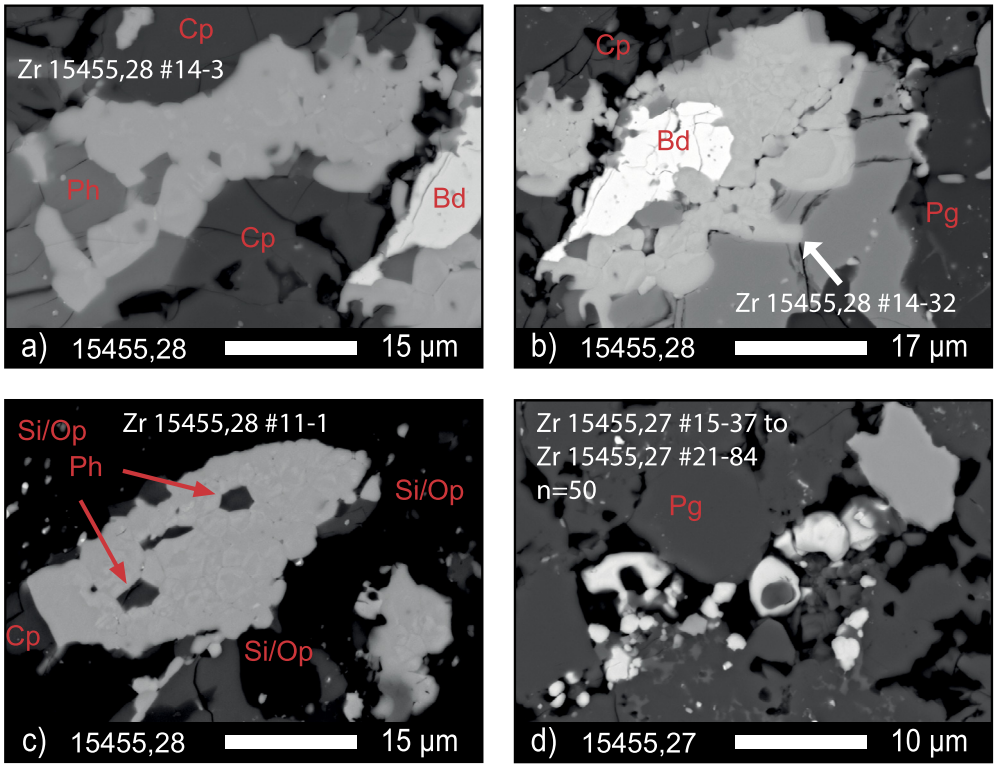

Fig. 2. BSE images of zircons from the dimict breccia 15455. Zircons occur predominantly as granular aggregates in the brecciated norite, but not in melt veins. a) Granular zircon aggregate enclosing phosphate (#14-3). b) Granular zircon aggregate (#14-32) partially replacing relic, fractured baddeleyite (see Fig. 1a). c) Poikilitic granular zircon aggregate (#11-1). The aggregate is enclosing phosphates and is associated with SiO_2 and orthopyroxene and likely formed by recrystallization of a coherent, poikilitic precursor grain. d) Elongate cluster of many small, subhedral and poikilitic zircon grains (n=50), located in a presumed former fracture of the norite. The aggregate may have formed from granular zircons (such as in a) which have been dispersed by shock-induced displacement and subsequent recrystallization as indicated by variations in brightness of their internal structure.

3. Results

Zircons occur in the impactites as small (mostly <10 µm), single grains, intergrowths of a few grains or granular aggregates of tiny (<1–2 µm) grains. QEMSCAN maps and BSE images show that zircons can be absent to abundant, with up to several tens or even hundreds of grains per section.

3.1. Zircon occurrence in relation to lithology

The occurrence and number of zircons appear to be often controlled by lithology. A QEMSCAN survey of different mono- and polymict lunar impactites shows that pristine noritic clasts often contain small zircons, whereas anorthositic impactites and their clasts often lack zircon or rarely contain zircon. In the pristine anorthositic norite clasts of 15455, granular zircon aggregates typically occur in 'evolved' silica-diopside rich domains or in the main norite along grain boundaries together with plagioclase, orthopyroxene and phosphates. The enstatite- and olivine-rich domain in 67955,48 contains abundant zircon, whereas the plagioclase rich domain in the section contains no zircon.

In the polymict impact breccia 67915 zircons occur in different types of clasts and in the fine-grained matrix, which also contains brown glass. The heterogeneity of clast lithologies is represented by the major element composition of plagioclase and mafic minerals, ranging from values typical for norites and anorthosites of the Magnesian suite to anorthosites of the Ferroan Anorthosite suite (Supplementary Fig. S2). The mineralogical mode of clasts as determined by QEMSCAN also displays this heterogeneity (Supplementary Figures S1 and S2). Zircons are abundant in noritic to troctolitic anorthosites and anorthosite clasts, which represent the most abundant clasts. Occasionally zircon also occurs in anorthositic gabbro, gabbroic anorthosite, noritic gabbro, anorthositic troctolite and gabbroic anorthosite clasts. In 67915, zircons are commonly associated with plagioclase, enstatite and troilite or occur in 'evolved' clasts intergrown with K-feldspar and SiO_2 (Fig. 1d) or both.

Zircons appear to be absent or rare in glass-rich or aphanitic, impact melt-dominated rocks such as KREEP rich melt rocks as indicated by QEMSCAN maps of sections 14310,19 and 67935,25. The same is observed for glass rich veins of impact melt, even if the veins are enriched in incompatible elements (e.g. the black veins in 15455).

3.2. Zircon textures and petrographic relations

Zircons occur in different textural variants in the impactites that are sometimes characteristic for a specific lithology or local mineral assemblage. Here, we present these in the order from the relatively simple breccias 15455 (Fig. 1a, 2) and 67955 (Fig. 1b, 3) to the more complex situation in the polymict breccia 67915 (Fig. 1c-d, 4). Zircons display five main modes of occurrence: (1) granular aggregates of tiny grains replacing pre-existing zirconium-phases (e.g. Fig. 2); (2) small subhedral to euhedral single grains or intergrown grains, typically on grain boundaries between main silicate minerals (Fig. 3, 4); (3) poikilitic to skeletal or conchoidal intergrowth of zircon with main silicate minerals (Fig. 3a, 4c, e); (4) anhedral zircon clasts in matrix (Fig. 4f) and (5) individual or groups of zircon grains associated with K-feldspar and/or SiO_2.

In 15455 granular zircon aggregates (referred to as 'granular zircons') are unfractured and commonly associated with diopside-silica domains, sometimes occurring with apatite and baddeleyite. Granular zircons comprise a few to several tens of tiny grains

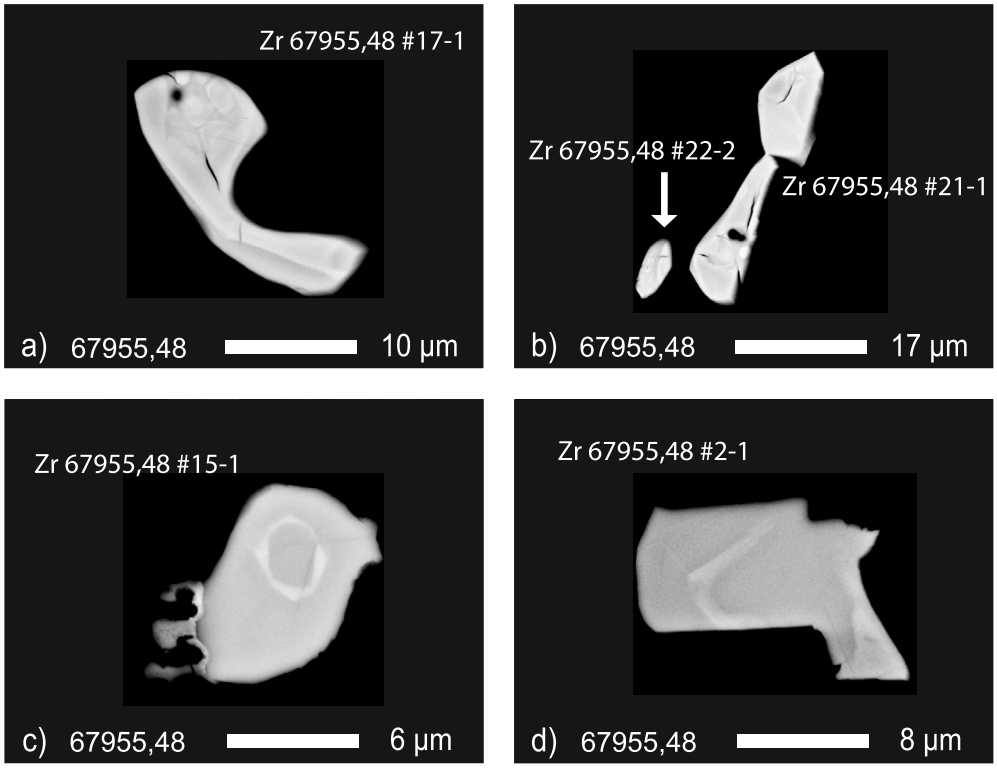

Fig. 3. BSE images of zircons from the dark domain of the brecciated impactite 67955,48. Because of the abundance of Fe-Ni metal and its chemical composition, the rock was interpreted as a cumulate crystallized from KREEP rich impact melt (Norman et al., 2016). Thus, zircons represent late crystallization products of the impact melt. a) BSE image of a subhedral, conchoidal zircon #17-1 showing granular internal structures (see also Fig. 1b). b) local group of subhedral zircon grains with a poikilitic grain. c-d) Subhedral zircons with domains of different brightness.

<2 µm with euhedral to subhedral shape (Fig. 2a-d). Sizes of the aggregates can be as small as 5 µm and may reach sizes as large as 38 µm by 61 µm. The aggregates sometimes are intergrown with baddeleyite (Fig. 2a, b) and interstitial regions between zircon neoblasts may contain SiO_2 rich glass. Aspect ratios and shapes of the granular zircons are suggestive of replacement of a previous generation of zircon or baddeleyite. Zircon aggregates may show different extents of granular recrystallization ranging from euhedral, spatially separate neoblasts (Fig. 2a, d) that formed by recrystallization of a larger coherent grain to textures in which recrystallized domains are merely recognizable by differences in brightness of BSE images (e.g. Fig. 2b, c). Granular textured zircons also occur in 67955 and in 67915, however, less frequently (e.g. Fig. 3a). Some granular zircon aggregates in 15455 enclose other mineral phases (e.g. apatite or plagioclase) and may represent recrystallized, formerly poikilitic textured zircons (see below). Clusters of zircon grains also occur in fractures and may represent formerly coherent zircon that may have recrystallized with subsequent displacement of the neoblasts. Some zircons within these clusters have a skeletal shape (Fig. 2d), or are poikilitically enclosing plagioclase.

In section 67955,48, zircon is mostly unfractured and occurs in the fine, fragmented 'matrix' and in noritic anorthosite clasts, which may also contain Fe-Ni metal and traces of K-feldspar. Zircons typically occur as single subhedral grains or groups of a few grains on grain boundaries with plagioclase and orthopyroxene (Fig. 3b-d, mean diameter is 4 µm). Some grains display embayed-conchoidal shapes or poikilitic textures (Fig. 3a, c, d), others show granular internal structures (Fig. 3a) or concentric light or dark irregular zones (Fig. 3c-d).

The polymict breccia 67915 contains variants of granular zircon and single zircon grains, similar to 15455 and 67955, however with a much greater diversity of clast compositions, mineral assemblages and zircon textures. Sections ,84 and ,76 differ somewhat in their clast assemblage and clast distribution (Supplementary Information 2.3). In both sections, zircon occurs in the Fe-Ni metal bearing matrix and in lithic clasts, some of which must represent older impactites because they are Fe-Ni metal bearing. Most zircons are subhedral to anhedral and occur with plagioclase, apatite and orthopyroxene. A significant fraction of K-feldspar and/or SiO_2 bearing clasts also host zircons (Fig. 4h) intergrown with either of these minerals (including Fe-Ni metal in one case). Typical zircon grain diameter is 6-8 µm. Some zircon grains reach sizes of up to 43 µm in width and 96 µm in length. Zircons either occur as single grains (Fig. 4a, b, f), in groups of grains (Fig. 4h) or as granular aggregates (Fig. 4d). Many grains are irregular and embayed (e.g. Fig. 4c). Poikilitic (e.g. Fig. 4b-c) to skeletal zircons (Fig. 4e) either occur in the matrix or in lithic clasts. Frayed zircons (e.g. Fig. 4g) have smoke like diffuse rims in BSE images. Examples of aggregates of granular zircon may contain tiny, bright inclusions, presumably representing baddeleyite (e.g. 4d, see also Crow et al., 2017). Some grains appear to have relict cores (e.g. Fig. 4a).

3.3. U-^{206}Pb and ^{207}Pb-^{206}Pb ages of zircons

Eleven analyses were obtained on seven grains from sections 15455,27 and ,28 (Table 1). To avoid inclusions of other phases, analyses were located in the cores or homogeneous areas of zircon aggregates. In some cases, spots were analyzed in less and more homogeneous domains of the same grain (Zr 15455,28 #11-1 and #14-32). Systematic variations of U-Th-Pb abundances regarding spot locations have not been observed. Uranium, Th and Pb mass fractions in zircons from 15455 range from 163 to 342, 55 to 231 and 229 to 729 µg/g, respectively. No ^{204}Pb signal was observed during these analyses. Analyses are concordant or reverse

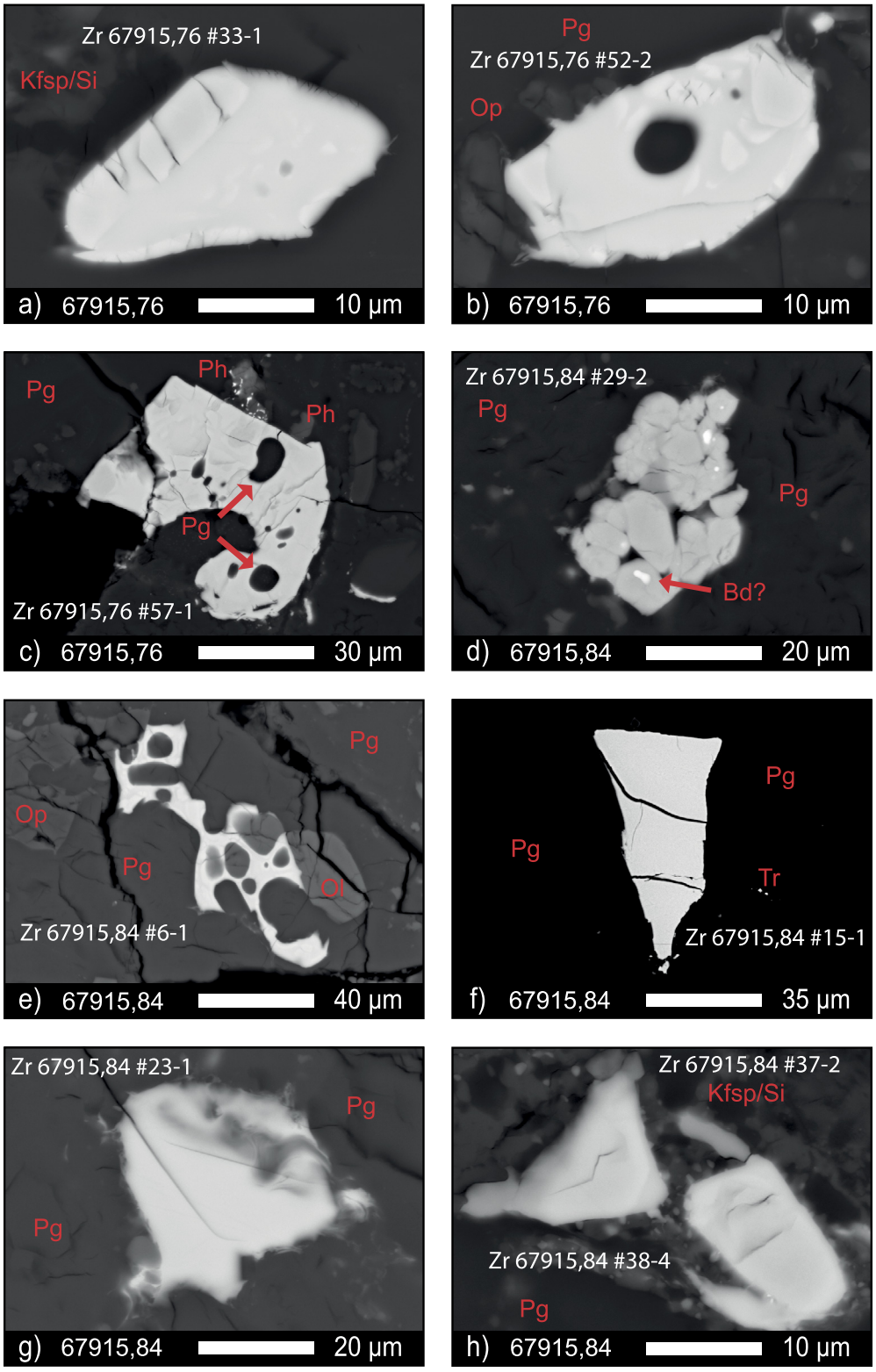

Fig. 4. BSE Images of zircons from the polymict breccia 67915. a) Subhedral zircon associated with K-feldspar (Kf) and SiO_2 (Si). The zircon shows attached relic (?) fractured zircon or baddeleyite on part of the rim of the grain. There are no fractures in the core, but patchy differences in brightness as in some other zircons (e.g. Fig. 4c). b) Poikilitic zircon showing patchy domains of brightness with plagioclase (Pg) and orthopyroxene (Op). c) Large fractured, partially poikilitic zircon enclosing plagioclase in association with phosphates (Ph). d) Granular zircon aggregate with bright baddeleyite (?, Bd) cores (compare Crow et al., 2017). e) Skeletal to poikilitic zircon enclosing plagioclase and olivine (Ol). f) Large fractured zircon clast. Tr: troilite. g) Subhedral, frayed zircon. h) Subhedral, locally frayed zircons in a K-feldspar and SiO_2 bearing clast.

discordant (Fig. 5a, see Supplementary Information 3). The coherence of the norite part and local textures suggest that the zircon grains we analyzed in 15455 are from the same source and have grown *in situ* in the norite lithology. Therefore, we also calculated an intercept age. Concordant analyses yield a mean concordia age of 4201 ± 11 Ma (2σ) while all data points with <80 % discordance yield an intercept age of 4206 ± 8 Ma (2σ), (Fig. 5a). The $^{207}Pb/^{206}Pb$ ages of all analyses of zircons from the present work

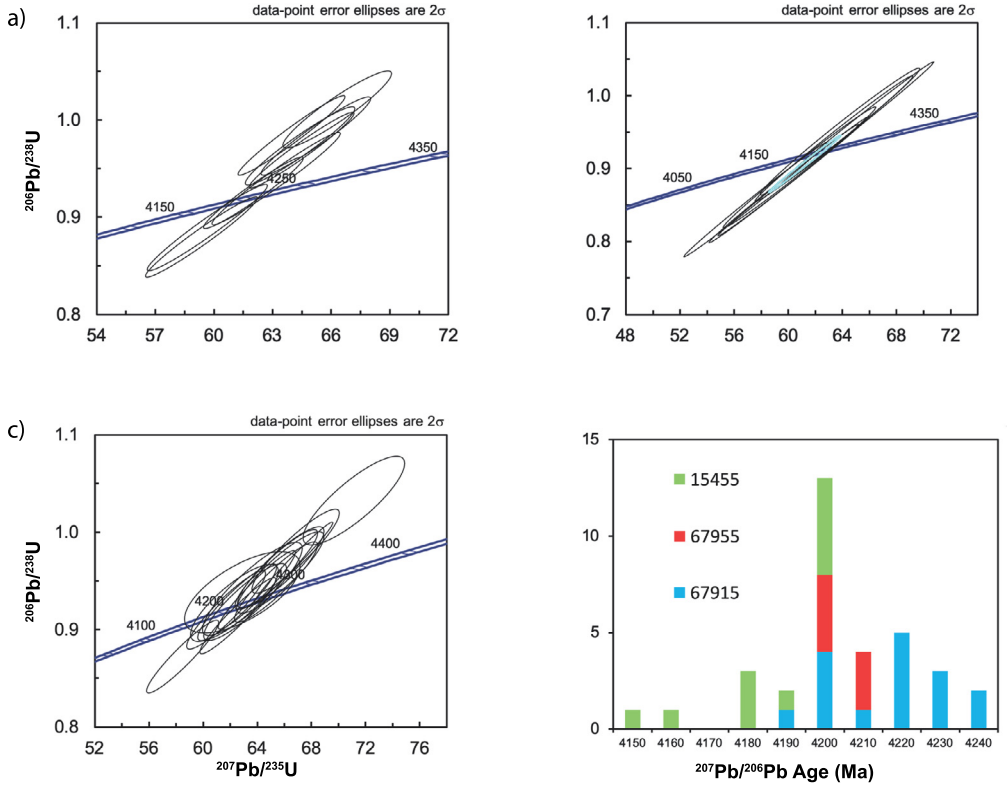

Fig. 5. U-Pb Concordia diagrams for zircon analyses in breccias 15455, 67955 and 67915 and distribution of $^{207}Pb/^{206}Pb$ ages (individual analyses). Note that 22 of the 24 zircons analyzed either are inferred to have crystallized from impact melt or show recrystallization textures. Whereas 67955 shows a unimodal distribution at 4.22 Ga, 67915 and 15455 show hints for the presence of ages that are somewhat older and somewhat younger than the prominent peak near 4.22 Ga.

on 15455 range from 4154 to 4210 Ma, with a weighted average of 4191 ± 4 Ma (2σ).

In 67955,48 four zircons from noritic and gabbroic anorthosite to anorthosite clasts and three zircons from the fragmented 'matrix' were analyzed (Table 2). Concentrations of U, Th and Pb in these zircons range from 119 to 465, 58 to 394 and 183 to 665 µg/g, respectively. Compared to zircons from clasts, zircons from the 'matrix' show generally higher concentrations of U, Th and Pb by a factor of ~2. The analyses show $^{204}Pb/^{206}Pb < 10^{-4}$, indicating insignificant initial lunar or terrestrial lead contamination. All analyses are concordant with a concordia age of 4211 ± 10 Ma 2σ (Fig. 5b) and agree well with a weighted average of all $^{207}Pb/^{206}Pb$ ages of 4211 ± 4 Ma 2σ. The full spectrum of $^{207}Pb/^{206}Pb$ ages ranges from 4202 to 4218 Ma (Fig. 5d) with all ages overlapping within their 2σ error and the weighted average.

In 67915 (Table 3), ten zircons were analyzed, including a large anhedral zircon clast in the matrix (Fig. 4f), a granular zircon aggregate, frayed zircon grains in the matrix, subhedral zircon from a K-Feldspar, SiO_2 and Fe-Ni metal bearing gabbroic anorthosite clast and poikilitic zircons in Fe-Ni metal bearing, noritic anorthosite clasts with variable proportions of K-feldspar. Three analyses have been performed on a poikilitic matrix zircon (35 µm, #57-1) that shows several mineral inclusions and irregular dark and light domains, suggesting different compositions. Zircon #57-1 displays the lowest U and Th concentrations in the darkest area of the BSE image compared to the other spots in this zircon (Table 1).

Mass fractions of U, Th and Pb in zircons from 67915 vary from 101 to 471, 44 to 379 and 159 to 778 µg/g, respectively. The $^{204}Pb/^{206}Pb$ ratio is $<3 \bullet 10^{-4}$ for all analyses. Most analyses are concordant (Fig. 5c), however some are reverse discordant and one is slightly discordant (−5%). A concordia intercept age yields 4216 ± 9 Ma (2σ) which agrees with a concordia age of 4231 ± 13 Ma (2σ) (concordant points only). The $^{207}Pb/^{206}Pb$ ages range from 4200 to 4241 Ma with a weighted average of 4225 ± 5 Ma (2σ).

4. Discussion

Our study provides some unexpected results, including the complete lack of zircon ages <4 Ga as well as the narrow age range of small zircon grains from different impactite (e.g. 15455, 67955) and clasts lithologies (67915). For a comparison of the U-Pb age results from zircons of the present study with previous results, it is necessary to identify and assess possible formation and recrystallization processes of zircons. In the following, we will use textural arguments, mineral assemblages and chemical information as well as analogues from terrestrial impact settings to infer the most plausible formation and modification processes of the zircons. Later, these arguments are combined with the age constraints.

4.1. Identification of impact-modified zircons

Zircons have been identified in all three samples. In principle, zircons might represent clasts of igneous zircons that formed during the presumed primary or secondary lunar magmatism, as has been suggested for studies of larger zircon grains, which typically show strong oscillatory zoning in their interiors (e.g. Nemchin et al., 2012). Igneous zircons may have recrystallized by impact-related heating or could have been partially reset by such processes (e.g. Crow et al., 2017). Here, we use the term 'impact zircon' for zircons that can be shown to have crystallized from impact melt or may have formed by partial or complete recrystallization caused by impact heating.

Former impact melt now occurs as clast bearing melt rocks, melt breccias and glass rich veins, e.g. in dimict breccias such as 15455 or veins in the matrix of 67955 and 67915. In order to decide if zircons recrystallized by impact-related heating or melting, or represent igneous clasts, we use zircon textures and the presence of Fe-Ni metal. The presence of Fe-Ni metal particles in clasts

Table 2
U-Th-Pb isotopic data of zircons of sample 67955,48.

Sample	Grain	Spot	U [ppm]	Th [ppm]	Pb [ppm]	238U/204Pb	238U/206Pb	±2σ (%)	204Pb/206Pb	±2σ (%)	207Pb/206Pb	±2σ (%)	207Pb*/206Pb	±2σ (%)	207Pb*/206Pb	±2σ (Ma)
67955,48	27-1	1	357	282	581	$4.98*10^{9}$	1.04	7.6	$2*10^{-10}$	200.0	0.4903	0.6	0.4903	0.6	4212	9
67955,48	16-1	1	119	58	183	$1.67*10^{5}$	1.05	7.5	$6*10^{-06}$	200.0	0.4868	1.1	0.487	1.1	4202	16
67955,48	2-1	1	425	179	641	$3.12*10^{5}$	1.06	7.5	$3*10^{-06}$	144.7	0.4885	0.8	0.4885	0.8	4207	12
67955,48	11-1	1	268	195	386	$6.94*10^{5}$	1.14	7.5	$2*10^{-06}$	200.0	0.4921	0.6	0.4921	0.6	4218	9
67955,48	21-1	1	192	124	280	$1.62*10^{4}$	1.11	7.5	$7*10^{-05}$	42.6	0.4896	0.9	0.4891	0.9	4209	13
67955,48	14-1	1	465	394	662	$4.70*10^{4}$	1.17	7.5	$2.5*10^{-05}$	57.7	0.4870	0.7	0.4868	0.7	4202	10
67955,48	15-1	1	450	378	665	$1.51*10^{4}$	1.12	7.5	$7.4*10^{-05}$	30.9	0.4926	0.6	0.4922	0.6	4218	8

* Common Pb corrected.

Table 3
U-Th-Pb isotopic data of zircons of samples 67915,84 and,76.

Sample	Grain	Spot	U [ppm]	Th [ppm]	Pb [ppm]	238U/204Pb	238U/206Pb	±2σ (%)	204Pb/206Pb	±2σ (%)	207Pb/206Pb	±2σ (%)	207Pb*/206Pb	±2σ (%)	207Pb*/206Pb	±2σ (Ma)
67915,84	15-1	1	103	57	164	$8.18*10^{3}$	1.02	3.6	$1.2*10^{-04}$	95.1	0.494	1.7	0.494	1.7	4225	24
67915,84	15-1	2	104	55	164	$1.11*10^{4}$	1.04	3.6	$9.4*10^{-05}$	79.0	0.497	1.9	0.497	1.9	4232	27
67915,84	15-1	3	104	58	162	$8.63*10^{3}$	1.05	3.5	$1.2*10^{-04}$	75.6	0.500	1.5	0.500	1.5	4241	22
67915,84	15-1	4	102	56	159	$7.48*10^{3}$	1.03	3.6	$1.4*10^{-04}$	96.1	0.495	1.8	0.495	1.8	4225	27
67915,84	16-4	1	471	379	777	$7.12*10^{4}$	1.03	3.5	$1.4*10^{-05}$	91.6	0.4991	0.6	0.4991	0.6	4239	9
67915,84	29-2	1	101	120	163	$1.19*10^{4}$	1.07	3.6	$9*10^{-05}$	200.0	0.486	4.2	0.486	4.2	4200	61
67915,84	37-2	1	112	44	187	$4.221*10^{3}$	0.97	3.6	$2.3*10^{-04}$	70.7	0.500	2.3	0.500	2.3	4241	34
67915,76	7-1	1	135	57	202	$1.12*10^{4}$	1.06	4.1	$9*10^{-05}$	137.4	0.490	2.3	0.490	2.3	4212	34
67915,76	31-1	1	229	75	334	$1.67*10^{5}$	1.08	3.5	$6*10^{-06}$	200.0	0.489	1.5	0.489	1.5	4207	22
67915,76	41-1	1	192	71	281	$1.08*10^{9}$	1.08	3.5	$1*10^{-09}$	200.0	0.487	2.4	0.487	2.4	4203	36
67915,76	43-1	1	332	149	514	$1.71*10^{4}$	1.04	3.5	$6*10^{-05}$	100.0	0.493	1.5	0.493	1.5	4221	23
67915,76	48-1	1	271	118	402	$1.08*10^{9}$	1.08	3.5	$1*10^{-09}$	200.0	0.493	1.9	0.493	1.9	4220	28
67915,76	48-1	2	248	84	360	$1.42*10^{4}$	1.09	3.6	$7.6*10^{-05}$	89.4	0.486	1.5	0.486	1.5	4200	22
67915,76	57-1	1	257	86	372	$2.45*10^{4}$	1.09	3.5	$4.5*10^{-05}$	94.6	0.496	1.1	0.496	1.1	4230	16
67915,76	57-1	2	388	186	543	$5.04*10^{4}$	1.15	3.5	$2*10^{-05}$	100.0	0.486	1.3	0.486	1.3	4200	19
67915,76	57-1	3	295	111	441	$6.38*10^{4}$	1.06	3.5	$2*10^{-05}$	137.5	0.493	1.1	0.493	1.1	4221	16

* Common Pb corrected.

and matrix are used to argue for or against meteoritic contamination of the host clast or the matrix. For instance, subhedral to euhedral zircon grains in clasts of coherent, Fe-Ni metal-bearing igneous rocks strongly suggest crystallization of these rocks and their zircons from impact melt (e.g. 67955; Norman et al., 2016). Delicate conchoidal, poikilitic or skeletal zircons (Fig. 3a, c; Fig. 4c, e) in Fe-Ni bearing clasts or matrix cannot have been preserved during transport and must have formed by *in situ* crystallization or recrystallization of previous zirconium-minerals caused by impact heating. In addition, existing information on specific rocks (e.g. the cumulate nature and HSE abundances of 67955, Norman et al., 2016) can be used to support the crystallization of zircons from impact melt.

The most evident impact-generated texture present in the three samples is represented by granular-textured zircons. Crow et al. (2017) mechanically separated two large granular zircon aggregates from breccia 15455 with individual grains of up to 20 µm size. The granular zircon aggregates show interstitial SiO_2 rich glass and small baddeleyite inclusions. These zircon aggregates are similar to the small granular zircon aggregates in 67915 (Fig. 4d). Some of the latter also contain tiny bright inclusions in BSE images that might represent baddeleyite. Most zircon neoblasts of granular zircons in 15455 from the present study are smaller with ~1 – 2 µm diameter or less. Compared to the large aggregates in Crow et al. (2017) they are often less well developed with less interstitial material between neoblasts, and neoblasts do not contain baddeleyite inclusions. Some of the granular zircon aggregates we identified in 15455 are similar to granular zircon aggregates observed by Thiessen et al. (2019) in breccia 14314 which also show small neoblasts. Transmission electron microscope studies show that variations in brightness of individual zircon neoblasts in BSE images result from variable crystallinity (Vanderliek et al., 2019).

Granular recrystallization of zircon has also been observed in terrestrial impactites and in metamorphic rocks that are not associated with impact events (Cavosie et al., 2015). Zircons recrystallized by impact-heating on Earth show unzoned neoblasts and yielded the age of the impact. FRIGN (former reidite in granular neoblastic) zircons have formed by the transition from zircon to reidite at high-pressures and subsequent high-temperature recrystallization to zircon or ZrO_2 and SiO_2 (e.g. Cavosie et al., 2018). The ~1 - 2 µm size of neoblasts of the present study match the size of neoblasts formed during shock stage IV observed by Schmieder et al. (2015) in terrestrial rocks. They also occur in ejecta deposits (Krogh et al., 1993) or suevitic and tektite glasses (Kleinmann and Letters, 1968). Some granular zircons may have formed at ultrahigh temperatures in crater floor environments of impact structures >250 km diameter (Moser et al., 2011; Crow et al., 2017).

In cases where zircon aggregates surround baddeleyite (Fig. 2b) the latter appears to be partially replaced by zircon neoblasts, showing crystal faces towards baddeleyite (see also Grange et al., 2009, 2013). Some granular zircons in 15455 and 67955 (Fig. 2c, 3a) show remnant poikilitic textures indicating in situ crystallization before granular recrystallization occurred and thus indicate a multi-stage evolution.

Poikilitic zircons in lunar impactites were interpreted to have formed during impact heating because textures suggest that they grew *in situ* (Liu et al., 2012; Grange et al., 2013; Thiessen et al., 2019). Late stage crystallization of zircon from interstitial impact melt pockets (Grange et al., 2013; Liu et al., 2009) or equilibrium crystallization from impact melt was proposed (Liu et al., 2012; Nemchin et al., 2008). However, the use of this texture alone as an unambiguous tracer for impact melt is debated (Osinski and Kring, 2015). Furthermore, it is not possible to distinguish between zircons that partially and completely enclose other mineral phases. Most zircon grains that appear poikilitic or skeletal in the present study occur in 67915. Zircons in clasts (Fig. 4e) or in the matrix (Fig. 4c) of this sample completely or partially enclose plagioclase, olivine and phosphates. Poikilitic zircons located in lithic clasts are less fractured and have a fresh appearance unlike those in the matrix which are commonly fractured. Due to the fragility of these zircons those that are unfractured must have crystallized *in situ* and cannot represent foreign mineral clasts in their host clasts (see also Grange et al., 2009). Some of these clasts also contain Fe-Ni particles and we therefore argue that poikilitic zircons associated with Fe-Ni metal have grown from interstitial impact melt. Poikilitic zircon grains in the Fe-Ni metal bearing matrix likely crystallized from local patches of impact melt soon after assemblage of the rock. Poikilitic zircons in the dark domain of 67955,48 (Fig. 3b) and disseminated Fe-Ni particles in clasts and matrix indicate that this sample crystallized from impact melt (see also Norman et al., 2016). Conchoidal grain shapes (Fig. 3a), imply that zircons in 67955 crystallized from local melt on grain boundaries, presumably due to highly localized zircon saturation, caused by kinetically-controlled growth processes. The internal granular texture of the grain in Fig. 3a suggests at least two heating events, the crystallization from impact melt and subsequent incipient recrystallization. Therefore, zircons in 67955 might record two different impact events.

Monomict zircon-bearing impactite clasts in 67915 are commonly noritic anorthosites, similar to the dark lithology of 67955,48. They also contain disseminated Fe-Ni particles and poikilitic zircons that, due to their fragility, would not have survived transport. Thus, these zircons must have grown *in situ* in the clasts, presumably during a previous impact-related melting event. These results show that poikilitic zircons commonly form during the rapid crystallization of impact melt in these lithologies.

Other zircons either represent clasts (Fig. 4f) or are of unclear origin because of unspecific textures and environments.

4.2. U-Pb zircon ages and impact-related heating

Of the 24 zircon grains dated in the present study, 22 show evidence that they were affected or formed by impact heating. The main constraints are (1) the occurrence in impact melt breccias or clasts (as indicated by Fe-Ni grains or HSE composition) with textural evidence for *in situ* growth and (2) partial or complete recrystallization features that, according to the previous discussion, were caused by impact heating (Supplementary Table S1–3). Previously determined Ar-Ar and U-Pb apatite ages for 15455, 67955 and 67915 scatter predominantly around ~3.9 Ga (Norman and Nemchin, 2014; Venkatesan and Alexander Jr., 1976; Alexander Jr. and Kahl, 1974; Bernstein, 1983; Kirsten et al., 1973)). In contrast, previous U-Pb data on large zircons show a large age range, typically from 4.0 to 4.35 Ga (Nemchin et al., 2012; Crow et al., 2017; Thiessen et al., 2019 and references therein). While many of the large zircons from previous work preserve igneous growth zoning, the small zircons (and a large zircon in 67915,84) of the present study do not show such evidence in cathodoluminescence images (see supplementary Figure S4). Another major difference is the lack of discordance in the small zircons, whereas discordance is more common among large lunar zircons.

The range of ^{207}Pb-^{206}Pb ages for small zircons in 15455 (4154 to 4210 Ma, Table 1) is rather narrow and shows no systematic relation with textural variations of zircons. A key objective of the present study was to test whether or not the U-Pb system of the small zircons might have been affected by nearby Imbrium impact melt veins. The apparent distances of such melt veins to dated zircons in the norite clasts range between ~120 and ~1200 µm. The mostly concordant U-Pb data of around 4.2 Ga show that even tiny recrystallized zircons were not affected strongly by subsequent impact heating. However, the spread of $^{207}Pb/^{206}Pb$ ages between 4154 and 4210 shows a resolvable age difference between some

zircons. Thus, it is likely that impact events younger than 4.2 Ga have affected the U-Pb system of the younger zircons in the sample. The small zircon grains are considerably younger than the 4.33 Ga age of the two large granular zircon aggregates of Crow et al. (2017) from the same rock, and because such ages do not occur in the present study, we infer that the large granular zircon may represent clasts from a different portion of the rock.

The presence of disseminated Fe-Ni particles observed in clasts and matrix of the brecciated domain in breccia 67955,48 indicates that this material crystallized from impact melt. Norman and Nemchin (2014) suggested that lithologies in 67955 may represent cumulates from KREEP bearing impact melt. The inferences from trace element modeling are consistent with the local occurrence of K-feldspar and phosphates in the dark domain, which may signify areas of trapped KREEP rich melt. Hence, zircon grains in 67955,48 are late crystallization products of differentiated impact melt on grain boundaries (see Figs. 3a, b). The narrow range of ^{207}Pb-^{206}Pb ages (4202-4218 Ma) of zircons with very different shapes in 67955,48 (Fig. 3) is consistent with a single event, which either may represent crystallization from the impact melt or heating by a subsequent impact event. Norman and Nemchin, 2014 obtained in situ ^{207}Pb-^{206}Pb ages of zirconolite and apatite in an unbrecciated, poikilitic lithology of 67955. Their oldest ^{207}Pb-^{206}Pb age obtained for low-U zirconolite (4220 $\pm$ 10 Ma) agrees well with the concordia age of the zircons (4211 $\pm$ 10 Ma). These ages are supported by a Sm-Nd isochron, which suggests that the ages indeed record the crystallization of the cumulate from impact melt (Norman et al., 2016). In contrast, high-U zirconolite and apatites yielded ages, ranging from 4.2 to 3.9 Ga (Norman and Nemchin, 2014) which was interpreted to reflect partial or complete resetting due to later impact heating. According to this interpretation, the different lithologies of 67955,48 may belong to the same cumulate sequence crystallized from a larger impact melt sheet at around ~4.22 Ga and have been fractured and welded together during later impacts, notably at ~3.9 Ga. As in 15455, the lack of response of the U-Pb system in the zircons to post 4.2 Ga heating processes is remarkable.

Poikilitic zircons in Fe-Ni metal bearing clasts of 67915 (Zr 67915,84 #41-1, #48-1) display overlapping ^{207}Pb-^{206}Pb ages of 4200 to 4220 Ma (n=4). A large, fractured poikilitic zircon in the matrix (Zr 67915,76 #57-1) records ages ranging from 4200 to 4230 Ma (n=3). These age ranges overlap within 2σ uncertainties and record at least one impact-related heating event that led to melting and formation of the poikilitic zircons. These results align with the age for a granular zircon (Zr 67915,84 #29-2) of 4200 Ma, which according to previous reasoning is impact related, and data for a skeletal grain (Zr 67915,76 #7-1) located in an Fe-Ni metal bearing clast that yields 4211 Ma. This coincidence of ages for very different types of zircons and local settings (clasts, matrix) in a polymict impactite suggests that the zircons crystallized during the same or multiple heating and melting events that occurred within the narrow time interval recorded by the U-Pb data. The similar ages also strengthen the argument that poikilitic zircon in clasts and matrix of impactites can be used to date impact events, provided that it can be shown that zircons crystallized from impact melt (e.g. nearby Fe-Ni, abundances of HSE). Some zircon grains in 67915 of uncertain origin tend to show systematically older ages between 4239 and 4241 Ma (Zr 67915,84 #15-1, Fig. 4f; Zr 67915,76 #16). The relative uniformity of zircon ages is remarkable, given the complex polymict nature of 67915 with a range of different clasts, however, the data show a hint for a bimodal distribution of ^{207}Pb-^{206}Pb ages (Fig. 5d). As for 15455 and 67955, there is no evidence for significant resetting of the U-Pb system in zircons by impact events post-dating 4.15 Ga.

Even though three very different samples from two landing sites were analyzed, including a complex polymict sample, the

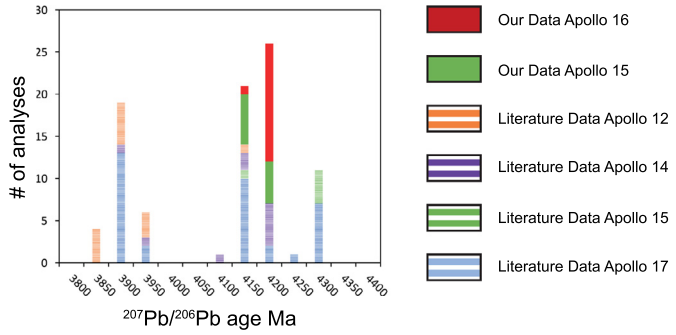

Fig. 6. ^{207}Pb/^{206}Pb ages from spot analyses of unambiguously impact related zircons extracted from literature. The data comprises in total 31 Apollo samples. For more details, including data sources, see Supplementary Figure S3.

^{207}Pb-^{206}Pb ages of all zircons combined only show a relatively narrow range between ~4150 and ~4250 Ma (Tables 1–3, Fig. 5). Although most of the ages overlap at the 2σ level, the distribution of the data hints that some zircons formed earlier than others with possible clusters at 4220 and 4240 Ma, and possibly a few younger zircons (Fig. 5d). Ages near 4.2 Ga were also reported from some presumably impact-modified larger zircons from other impactites (e.g. Crow et al., 2017; Pidgeon et al., 2007 and references therein).

4.3. Age distributions and their significance

In order to assess the current U-Pb age data on lunar zircons, we compiled >1000 zircon spot analyses from the literature and, using criteria explained before, grouped them into presumed, impact-related zircons, igneous zircons and zircons of uncertain origin (Supplementary Figure S5). For more than half of the published zircon data, information on their genesis (igneous or impact origin) was unclear. In Fig. 6, we only include grains of unambiguously impact-related origin (see also Crow et al., 2017). Granular, poikilitic (including irregular or skeletal shapes), and embayed textures were included, if additional information (e.g. presence of metal) was available. In addition, we included acicular grains and core-recrystallized rim textures. The larger data set now available supports the conclusion of (Crow et al., 2017) that major impact events occurred at ~4.3 Ga, ~4.2 Ga and ~3.9 Ga.

Recently Joy et al., 2020 dated zircons in regolith breccia 65745,7 showing ages ranging from 3.5 to 4.1 Ga. These grains have been interpreted to have undergone partial to complete resetting by the Imbrium impact and a later impact event at ~3.4 Ga. Thus, by including the new data for Apollo 16 samples it is clear that zircons at most landing sites have been affected by impact events between 3.9 and 4.33 Ga (e.g. Crow et al., 2017; Joy et al., 2020 and this work). All landing sites clearly show at least two impact-related zircon age populations. Because in many studies the U-Pb zircon ages do not record the 3.9 Ga event(s), which however is omnipresent among K-Ar and Rb-Sr dates (the main argument for a late lunar cataclysm), it is evident that the different response of geochronometers to late heating events plays a major role in how ages are distributed (e.g. Liu et al., 2020; Michael et al., 2018; Norman and Nemchin, 2014; Fernandes et al., 2013 and Supplementary Figure S5). Abundant K-Ar and Rb-Sr dates near ~3.9 Ga are a plausible consequence of the resetting by hot Imbrium ejecta (Hartmann, 1975). On the other hand, the robustness of the U-Pb system in zircon suggests that impact events capable of effectively resetting zircon were more widespread between 4.15 and 4.25 Ga than at any later time in lunar history. These observations are difficult to reconcile with the hypothesis of a late lunar cataclysm. Identical ages at different landing sites are explicable if some zircons formed and older zircons completely recrystallized by basin-forming impacts and were subsequently dispersed by later

impacts (e.g. Liu et al., 2020). Thus, the pre-4 Ga ages and effective zircon recrystallization at 4.2 Ga are more easily reconciled with the model of exponential decay of large impact events on the moon as proposed by Neukum and Ivanov, 1994. The source basins of the 4.2 Ga events are unknown. However, the ^{207}Pb-^{206}Pb age range of these zircons overlaps with crater counting ages of some large nearside basins, notably Nectaris and Serenitatis (Orgel et al., 2018; Neukum and Ivanov, 1994).

5. Summary and conclusions

Combining mineralogical mapping at high-spatial resolution, SEM imaging and U-Pb dating by SIMS allows to identify and analyze zircons as small as 6 µm, which were overlooked in previous studies of lunar impactites. Textures and petrogenetic context of 24 zircons (22 impact-related) from three samples of the Apollo 15 and 16 landing sites were studied and dated. Granular zircon aggregates recrystallized from pre-existing zirconium-phases. Some precursor zircon presumably derived from the local reaction of baddeleyite with silica rich melt produced by impact heating. Poikilitic or skeletal zircons in matrix or clasts likely crystallized from impact melt, as inferred from textures, rock composition or the presence of Fe-Ni particles. Many zircon analyses are concordant and show Pb-Pb ages with a limited range from 4.15 to 4.25 Ga. A surprising result is the absence of ages <4.1 Ga, which indicates the robustness of the U-Pb system in small zircons towards later impact heating events. The distribution of ages for impact-generated zircons in this study and from the literature (e.g. Crow et al., 2017) strengthens the hypothesis that several large impact events must have occurred on the Moon prior to 4.1 Ga.

CRediT authorship contribution statement

Dennis Marcel Vanderliek: Conceptualization, Data curation, Investigation, Methodology, Visualization, Writing – original draft. **Harry Becker:** Conceptualization, Funding acquisition, Project administration, Resources, Supervision, Writing – original draft. **Alexander Rocholl:** Methodology, Resources, Supervision, Writing – original draft.

Declaration of competing interest

The authors declare that they have no known competing financial interests or personal relationships that could have appeared to influence the work reported in this paper.

Acknowledgements

We thank NASA CAPTEM and Ryan Zeigler for providing lunar thin sections. We also would like to thank L. Gronen for the processing of QEMSCAN data, S. Weitkamp and T. Carl for sample imaging and processing M. Wiedenbeck for discussion and F. Couffignal for his excellent handling of the SIMS. Furthermore, we would like to thank W. McKinnon for editorial handling and A. Nemchin and C. Crow for their reviews. Funded by the Deutsche Forschungsgemeinschaft (DFG, German Research Foundation) – Project-ID 263649064 – TRR 170. This is TRR 170 Publication No. 145.

Appendix A. Supplementary material

Supplementary material related to this article can be found online at https://doi.org/10.1016/j.epsl.2021.117216.

References

Alexander Jr., E.C., Kahl, S., 1974. Ar-40/Ar-39 studies of lunar breccias. In: Lunar and Planetary Science Conference Proceedings, pp. 1353–1373.
Bellucci, J., Whitehouse, M.J., Nemchin, A., Snape, J., Pidgeon, R., Grange, M., Reddy, S., Timms, N., 2016. A scanning ion imaging investigation into the micron-scale U-Pb systematics in a complex lunar zircon. Chem. Geol. 438, 112–122.
Bernstein, M., 1983. 15445 and 15455: origin and preliminary age data. Lunar Planet. Sci. 14, 33–34.
Borg, L.E., Gaffney, A.M., Shearer, C.K., 2015. A review of lunar chronology revealing a preponderance of 4.34–4.37 Ga ages. Meteorit. Planet. Sci. 50, 715–732.
Butler, P., 1972. Apollo 16 Lunar sample information catalog. In: NASA (Ed.), MSC-03210. Lyndon B. Johnson Space Center, Houstion, Texas.
Cavosie, A.J., Erickson, T.M., Timms, N.E., Reddy, S.M., Talavera, C., Montalvo, S.D., Pincus, M.R., Gibbon, R.J., Moser, D.J.G., 2015. A terrestrial perspective on using ex situ shocked zircons to date lunar impacts. Geology 43, 999–1002.
Cavosie, A.J., Timms, N.E., Ferrière, L., Rochette, P., 2018. FRIGN zircon—the only terrestrial mineral diagnostic of high-pressure and high-temperature shock deformation. Geology 46, 891–894.
Cherniak, D., Watson, E., 2001. Pb diffusion in zircon. Chem. Geol. 172, 5–24.
Crow, C.A., McKeegan, K.D., Moser, D.E., 2017. Coordinated U–Pb geochronology, trace element, Ti-in-zircon thermometry and microstructural analysis of Apollo zircons. Geochim. Cosmochim. Acta 202, 264–284.
Fernandes, V., Fritz, J., Weiss, B., Garrick-Bethell, I., Shuster, D.J.M., Science, P., 2013. The bombardment history of the Moon as recorded by 40Ar-39Ar chronology. Meteorit. Planet. Sci. 48, 241–269.
Grange, M., Nemchin, A., Pidgeon, R., Timms, N., Muhling, J., Kennedy, A.J., 2009. Thermal history recorded by the Apollo 17 impact melt breccia 73217. Geochim. Cosmochim. Acta 73, 3093–3107.
Grange, M., Nemchin, A., Timms, N., Pidgeon, R., Meyer, C.J., 2011. Complex magmatic and impact history prior to 4.1 Ga recorded in zircon from Apollo 17 South Massif aphanitic breccia 73235. Geochim. Cosmochim. Acta 75, 2213–2232.
Grange, M., Pidgeon, R., Nemchin, A., Timms, N.E., Meyer, C.J., 2013. Interpreting U–Pb data from primary and secondary features in lunar zircon. Geochim. Cosmochim. Acta 101, 112–132.
Gronen, L.H., Sindern, S., Katzmarzyk, J.L., Bormann, U., Hellmann, A., Wotruba, H., Meyer, F.M., 2019. Mineralogical and chemical characterization of Zr-REE-Nb Ores from Khalzan Buregtei (Mongolia)—approaches to more efficient extraction of rare metals from alkaline granitoids. Minerals 9, 217.
Hartmann, W.K., 1975. Lunar "cataclysm": a misconception? Icarus 24, 181–187.
Hiess, J., Condon, D.J., McLean, N., Noble, S.R., 2012. 238U/235U systematics in terrestrial uranium-bearing minerals. Science 335 (6076), 1610–1614.
Joy, K.H., Snape, J., Nemchin, A., Tartèse, R., Martin, D., Whitehouse, M.J., Vishnyakov, V., Pernet-Fisher, J.F., Kring, D.A., 2020. Timing of geological events in the lunar highlands recorded in shocked zircon-bearing clasts from Apollo 16. R. Soc. Open Sci. 7, 200236.
Kirsten, T., Horn, P., Kiko, J., 1973. 39Ar-40Ar dating and rare gas analysis of Apollo 16 rocks and soils. In: Lunar and Planetary Science Conference Proceedings, p. 1757.
Kleinmann, B.J.E., Letters, P.S., 1968. The breakdown of zircon observed in the Libyan Desert Glass as evidence of its impact origin. Earth Planet. Sci. Lett. 5, 497–501.
Krogh, T., Kamo, S., Bohor, B., 1993. Fingerprinting the K/T impact site and determining the time of impact by UPb dating of single shocked zircons from distal ejecta. Earth Planet. Sci. Lett. 119, 425–429.
Lindstrom, M.M., Marvin, U.B., Vetter, S.K., Shervais, J.W., 1988. Apennine front revisited-diversity of Apollo 15 highland rock types. In: Lunar and Planetary Science Conference Proceedings, pp. 169–185.
Liu, D., Jolliff, B., Zeigler, R., Wan, Y., Zhang, Y., Dong, C., Korotev, R., 2010. A 3.91 billion year age for Apollo 12 High-Thorium impact-melt breccias: products of imbrium, or an older impact basin in the procellarum KREEP Terrane? In: Lunar and Planetary Science Conference, p. 2477.
Liu, D., Jolliff, B.L., Zeigler, R.A., Korotev, R.L., Wan, Y., Xie, H., Zhang, Y., Dong, C., Wang, W.J.E., Letters, P.S., 2012. Comparative zircon U–Pb geochronology of impact melt breccias from Apollo 12 and lunar meteorite SaU 169, and implications for the age of the Imbrium impact. Earth Planet. Sci. Lett. 319, 277–286.
Liu, D., Wan, Y., Zhang, Y., Dong, C., Jolliff, B., Zeigler, R., Korotev, R., 2009. Age of zircons in the impact-melt breccia in SaU 169 lunar meteorite: Beijing SHRIMP II study. In: Lunar and Planetary Science Conference.
Liu, J., Sharp, M., Ash, R.D., Kring, D.A., Walker, R.J., 2015. Diverse impactors in Apollo 15 and 16 impact melt rocks: Evidence from osmium isotopes and highly siderophile elements. Geochim. Cosmochim. Acta 155, 122–153.
Liu, T., Michael, G., Wünnemann, K., Becker, H., Oberst, J., 2020. Lunar megaregolith mixing by impacts: spatial diffusion of basin melt and its implications for sample interpretation. Icarus 339, 113609.
Ludwig, K.J., 2011. Isoplot v. 4.15: A Geochronological Toolkit for Microsoft Excel. Berkeley Geochronology Center. Special Publication 4, 75.
Marti, K., Aeschlimann, U., Eberhardt, P., Geiss, J., Grögler, N., Jost, D., Laul, J., Ma, M.S., Schmitt, R., Taylor, G.J., 1983. Pieces of the ancient lunar crust: ages and composition of clasts in consortium breccia 67915. J. Geophys. Res., Solid Earth 88.

Meyer, C., 2005. Lunar sample compendium.
Meyer, C., Williams, I.S., Compston, W., 1996. Uranium-lead ages for lunar zircons: evidence for a prolonged period of granophyre formation from 4.32 to 3.88 Ga. Meteorit. Planet. Sci. 31, 370–387.
Michael, G., Basilevsky, A., Neukum, G.J.I., 2018. On the history of the early meteoritic bombardment of the Moon: was there a terminal lunar cataclysm? Icarus 302, 80–103.
Moser, D., Cupelli, C., Barker, I., Flowers, R., Bowman, J., Wooden, J., Hart, J.J., 2011. New zircon shock phenomena and their use for dating and reconstruction of large impact structures revealed by electron nanobeam (EBSD, CL, EDS) and isotopic U–Pb and (U–Th)/He analysis of the Vredefort dome. Can. J. Earth Sci. 48, 117–139.
Nemchin, A., Grange, M., Pidgeon, R., Meyer, C., 2012. Lunar zirconology. Aust. J. Earth Sci. 59, 277–290.
Nemchin, A., Pidgeon, R., Healy, D., Grange, M., Whitehouse, M., Vaughan, J., 2009. The comparative behavior of apatite-zircon U-Pb systems in Apollo 14 breccias: implications for the thermal history of the Fra Mauro formation. Meteorit. Planet. Sci. 44, 1717–1734.
Nemchin, A., Pidgeon, R., Whitehouse, M., Vaughan, J.P., Meyer, C.J., 2008. SIMS U–Pb study of zircon from Apollo 14 and 17 breccias: implications for the evolution of lunar KREEP. Geochim. Cosmochim. Acta 72, 668–689.
Neukum, G., Ivanov, B., 1994. Crater size distributions and impact probabilities on Earth from lunar, terrestrial-planet, and asteroid cratering data. In: Hazards Due to Comets 1, pp. 359–416.
Norman, M., Duncan, R.A., Huard, J.J., 2010. Imbrium provenance for the Apollo 16 Descartes terrain: Argon ages and geochemistry of lunar breccias 67016 and 67455. Geochim. Cosmochim. Acta 74, 763–783.
Norman, M., Taylor, L.A., Shih, C.-Y., Nyquist, L., 2016. Crystal accumulation in a 4.2 Ga lunar impact melt. Geochim. Cosmochim. Acta 172, 410–429.
Norman, M.D., Nemchin, A., 2014. A 4.2 billion year old impact basin on the Moon: U–Pb dating of zirconolite and apatite in lunar melt rock 67955. Earth Planet. Sci. Lett. 388, 387–398.
Orgel, C., Michael, G., Fassett, C.I., van der Bogert, C.H., Riedel, C., Kneissl, T., Hiesinger, H., 2018. Ancient bombardment of the inner solar system: reinvestigation of the "fingerprints" of different impactor populations on the lunar surface. J. Geophys. Res., Planets 123, 748–762.
Osinski, G.R., Kring, D.A., 2015. Large Meteorite Impacts and Planetary Evolution V. Geological Society of America.
Pidgeon, R.T., Nemchin, A., Van Bronswijk, W., Geisler, T., Meyer, C., Compston, W., Williams, I.J., 2007. Complex history of a zircon aggregate from lunar breccia 73235. Geochim. Cosmochim. Acta 71, 1370–1381.
Roedder, E., Weiblen, P.W., 1974. Petrology of clasts in lunar breccia 67915. In: Lunar and Planetary Science Conference Proceedings, pp. 303–318.
Ryder, G., Bower, J., 1977. Petrology of Apollo 15 black-and-white rocks 15445 and 15455-fragments of the Imbrium impact melt sheet. In: Lunar and Planetary Science Conference Proceedings, pp. 1895–1923.
Ryder, G., Wood, J., 1977. Serenitatis and Imbrium impact melts: implications for lunar crustal composition and stratigraphy. In: Lunar and Planetary Science Conference.
Ryder, G., 2002. Mass flux in the ancient Earth-Moon system and benign implications for the origin of life on Earth. J. Geophys. Res., Planets 107, 6–1–6-13.
Schmieder, M., Tohver, E., Jourdan, F., Denyszyn, S., Haines, P.J., 2015. Zircons from the Acraman impact melt rock (South Australia): shock metamorphism, U–Pb and 40Ar/39Ar systematics, and implications for the isotopic dating of impact events. Geochim. Cosmochim. Acta 161, 71–100.
Shih, C.-Y., Nyquist, L., Dasch, E., Bogard, D., Bansal, B., Wiesmann, H.J., 1993. Ages of pristine noritic clasts from lunar breccias 15445 and 15455. Geochim. Cosmochim. Acta 57, 915–931.
Sindern, S., Meyer, F.M., 2017. Automated quantitative rare Earth elements mineralogy by scanning electron microscopy. In: Handbook of Rare Earth Elements - I Analytics, vol. 1. De Gruyter, pp. 334–356.
Stacey, J.t., Kramers, J., 1975. Approximation of terrestrial lead isotope evolution by a two-stage model. Earth Planet. Sci. Lett. 26, 207–221.
Stöffler, D., Ryder, G., Ivanov, B.A., Artemieva, N.A., Cintala, M.J., Grieve, R.A.J., 2006. Cratering history and lunar chronology. Rev. Mineral. Geochem. 60, 519–596.
Taylor, G., Warner, R., Keil, K., Ma, M.-S., Schmitt, R., 1980. Silicate liquid immiscibility, evolved lunar rocks and the formation of KREEP. In: Lunar Highlands Crust, pp. 339–352.
Tera, F., Papanastassiou, D., Wasserburg, G.J.E., Letters, P.S., 1974. Isotopic evidence for a terminal lunar cataclysm. Earth Planet. Sci. Lett. 22, 1–21.
Thiessen, F., Nemchin, A., Snape, J., Bellucci, J., Whitehouse, M.J., 2018. Apollo 12 breccia 12013: impact-induced partial Pb loss in zircon and its implications for lunar geochronology. Geochim. Cosmochim. Acta 230, 94–111.
Thiessen, F., Nemchin, A., Snape, J., Whitehouse, M.J., 2019. U-Pb SIMS ages of Apollo 14 zircon: Identifying distinct magmatic episodes. Meteorit. Planet. Sci. 54, 1720–1736.
Vanderliek, D.M., Kusiak, M.A., Wirth, R., Becker, H., Rocholl, A., 2019. Origin of Granular Zircon in Lunar Impactites. Geomünster.
Venkatesan, T., Alexander Jr., E., 1976. 40Ar-39Ar study of a clasts 12-1 from 67915. In: Lunar and Planetary Science Conference.
Warren, P., Wasson, J., 1979. The compositional-petrographic search for pristine nonmare rocks-third foray. In: Lunar and Planetary Science Conference Proceedings, pp. 583–610.
Wiedenbeck, M., Alle, P., Corfu, F., Griffin, W., Meier, M., Oberli, F., v. Quadt, A., Roddick, J., Spiegel, W., 1995. Three natural zircon standards for U-Th-Pb, Lu-Hf, trace element and REE analyses. Geostand. Newsl. 19, 1–23.